Reaction dynamics of the 4-methylphenyl radical ($C_6H_4CH_3$; *p*-tolyl) with isoprene (C_5H_8) – formation of dimethyldihydronaphthalenes†

Beni B. Dangi,[a] Tao Yang,[a] Ralf I. Kaiser*[a] and Alexander M. Mebel*[b]

We probed the reaction of the 4-methylphenyl radical with isoprene under single collision conditions at a collision energy of 58 kJ mol⁻¹ by exploiting the crossed molecular beam technique. Supported by the electronic structure calculations, the reaction was found to initially lead to a van-der-Waals complex without any barrier which can then isomerize by addition of the 4-methylphenyl radical to any one of the four carbon atoms of the 1,3-butadiene moiety of isoprene. The initial addition products isomerize with formal addition products preferentially to C1 and C4 carbon atoms of the isoprene. These structures further isomerize *via* hydrogen migration and cyclization; the reaction is terminated by a hydrogen atom elimination from the 4-methylphenyl moiety *via* tight exit transition states leading to two dimethyl-dihydronaphthalene isomers as the dominating products. This study presents one of the very first bimolecular reactions of the 4-methylphenyl radical with unsaturated hydrocarbons and opens a path for the investigation of this reaction class in future experiments.

1. Introduction

During the last few decades, polycyclic aromatic hydrocarbons (PAHs) and related compounds such as (de)hydrogenated and/or alkyl substituted PAHs have received significant interest from the combustion,[1] atmospheric,[2] and interstellar[3] chemistry communities. In the interstellar medium (ISM), PAH-like species are suggested to account for up to 20% of the cosmic carbon budget[3] and have been proposed as the carriers of the diffuse interstellar bands (DIBs)[4] and of the unidentified infrared (UIR)[5] emission bands. Likely formed in outflows of dying carbon stars such as IRC+10216, PAHs have also been contemplated as critical reaction intermediates leading to carbonaceous nano-particles (interstellar dust).[6] On Earth, PAHs are predominantly formed by incomplete combustion of fossil fuels, are considered as acute atmospheric and water pollutants due to their adverse health effects acting as mutagens and carcinogens,[7] and are linked to the formation of soot particles. Commonly referred to as carbonaceous nanoparticles, soot is primarily composed of nanometer-sized stacks of perturbed graphitic layers that are oriented concentrically in an onion-like fashion.[8] These layers can be characterized as fused benzene rings and are likely formed *via* agglomeration of polycyclic aromatic hydrocarbons.[9] These carbonaceous nanoparticles are emitted to the atmosphere from natural and anthropogenic sources with an average global emission rate of anthropogenic carbon from fossil fuel combustion as high as 2.4×10^{10} kg per year.[10] Once liberated into the ambient environment, soot particles in respirable size of 10–100 nm can be transferred into the lungs by inhalation[11] and are strongly implicated in the degradation of human health,[12] particularly due to their high carcinogenic risk potential. PAHs and carbonaceous nanoparticles are also serious water pollutants of marine ecosystems[13] and bio-accumulate in the fatty tissue of living organisms.[14] Together with leafy vegetables, where PAHs and soot deposit easily, they have been further linked to soil contamination,[15] food poisoning, liver lesions, and tumor growth. Soot particles with diameters of up to 500 nm can be transported to high altitudes[16] and influence the atmospheric chemistry.[17] These particles act as condensation nuclei for water ice, accelerate the degradation of ozone, change the Earth's radiation budget,[18] and could lead ultimately to an increased rate of skin cancer on Earth[19,20] and possibly to a reduced harvest of crops.[21]

The underlying mechanisms of PAH formation and growth in hydrocarbon flames and in combustion engines are very complex. Kinetic models of flames are often exploited to propose likely reaction mechanisms of how PAHs and ultimately soot might be formed.[22] In such systems, the synthesis of the very first mono-cyclic aromatic structures such as the phenyl radical (C_6H_5) and benzene (C_6H_6) is suggested to be the rate determining step in

[a] Department of Chemistry, University of Hawai'i at Manoa, Honolulu, HI 96822, USA. E-mail: ralfk@hawaii.edu

[b] Department of Chemistry and Biochemistry, Florida International University, Miami, FL 33199, USA. E-mail: mebela@fiu.edu

† Electronic supplementary information (ESI) available. See DOI: 10.1039/c4cp01056f

This journal is © the Owner Societies 2014

Phys. Chem. Chem. Phys., 2014, **16**, 16805–16814 | **16805**

the mass growth processes.[22–24] The formation of polycyclic aromatic hydrocarbons carrying (alkyl-substituted) five-membered rings is of particular interest,[25–27] since these molecules are likely involved in PAH growth producing non-planar bowl-shaped structures such as corannulene.[28] Even though flame studies are able to propose *likely* combustion mechanisms, it is often difficult to draw definite mechanistic conclusions from these investigations due to the occurrences of complex parallel and sequential chemical reactions leading often to the same reaction product and/or structural isomers. Hence, only the detailed investigation of individual reactions at the microscopic level can help to fully understand the complex reactions involved in the combustion process.

A systematic investigation of bimolecular reactions of unsaturated hydrocarbon molecules with aromatic radicals – namely the phenyl radical – under single-collision conditions has been conducted in our laboratory during the last few years. More specifically, indene (C_9H_8),[29] naphthalene ($C_{10}H_8$),[30] and 1,4-dihydronaphthalene ($C_{10}H_{10}$)[31] were formed *via* bimolecular reactions of the phenyl radical (C_6H_5) with allene/methylacetylene (C_3H_4), vinylacetylene (C_4H_4), and 1,3-butadiene (C_4H_6), respectively (Fig. 1). The related aromatic radical – methylphenyl ($C_6H_4CH_3$) – presents the simplest alkyl-substituted phenyl radical; this species poses also an isomer of the benzyl radical ($C_6H_5CH_2$), which is abundant in combustion flames. Zhang *et al.* detected the benzyl radical *via* pyrolysis of toluene through photoionization molecular beam mass spectrometry and proposed its crucial role in the hydrocarbon growth process.[32] Due to their importance as reaction intermediates in hydrocarbon growth and soot formation, the potential energy surfaces (PESs) of the C_7H_7 radicals – benzyl ($C_6H_5CH_2$), *o*-, *m*-, and *p*-tolyl (or 2-, 3-, and 4-tolyl) ($C_6H_4CH_3$), and cycloheptatrienyl (C_7H_7) – have been explored extensively.[32,33] The benzyl radical is the most studied C_7H_7 isomer reporting kinetics and products with several combustion-relevant species such as atomic hydrogen (H),[34,35] nitrogen monoxide (NO),[36] molecular oxygen (O_2),[36,37] hydroxyl radical (OH),[38] and methyl radical (CH_3).[39,40] The reaction of the C_7H_7 radical with the methyl radical producing styrene (C_8H_8) and molecular hydrogen was reported by Smith.[41] The reaction of C_7H_7 (benzyl) with hydrogen iodide (HI) was performed exploiting the *very low pressure pyrolysis* technique to determine the rate constant and the enthalpy of formation of the benzyl radical.[42] Reactions of methylphenyl radicals with molecular oxygen[43] and deuterium[44] have also been reported.[45] Note that da Silva *et al.* presented theoretical results on the reactions of methylphenyl radicals with molecular oxygen and ethylene.[43] Unfortunately, reactions of *any* C_7H_7 isomer with unsaturated hydrocarbons under single collision conditions have been elusive.

In this paper, we report the preparation of the 4-methylphenyl (4-tolyl) radical *via* 193 nm photodissociation of 4-chlorotoluene and present the first results from the crossed molecular beam reactions with 2-methyl-1,3-butadiene (isoprene) leading to the formation of two isomers of dimethyldihydronaphthalene.

2. Methods

2.1. Experimental and data analysis

The experiments were conducted under single collision conditions utilizing a universal crossed molecular beam machine described elsewhere.[46,47] Briefly, a pulsed supersonic beam of 4-tolyl radicals ($C_6H_4CH_3$) was generated *via* photodissociation of 4-chlorotoluene ($C_6H_4CH_3Cl$; 98%; Sigma-Aldrich) seeded in helium (99.9999%; Airgas Gaspro) at fractions of about 0.2%. The gas mixture was expanded through a Proch–Trickl pulsed valve with a 0.96 mm nozzle diameter operating at repetition rates of 120 Hz and opening times of 80 µs. After the expansion, the 4-chlorotoluene precursor was photodissociated at 193 nm, a 60 Hz repetition rate, and pulse energies of 10 ± 2 mJ (Compex 110 Excimer laser, Lambda Physik). The laser output was focused by a 1.5 m quartz focus lens to a 4 mm × 1 mm rectangle before it intercepted the molecular beam perpendicularly 1 mm downstream of the nozzle. The helium gas backing pressure of 1.8 atm resulted in a pressure of about 2×10^{-4} Torr in the primary source chamber. The molecular beam then passed a skimmer and a four-slot chopper wheel, which selected a segment of the pulsed 4-tolyl radical beam of a well-defined peak velocity (v_p) and a speed ratio (S) (Table 1). This segment of the pulsed 4-tolyl beam then crossed a pulsed isoprene beam (C_5H_8, 99%, TCI America) perpendicularly in the interaction region. The pulsed isoprene beam was generated by a second pulsed valve operating at a backing pressure of 480 Torr and a repetition rate of 120 Hz thus yielding a pressure of about 1×10^{-4} Torr in the secondary source chamber. A photo diode mounted on top of the chopper wheel provided the time zero of the experiments. It is important to note that the 4-tolyl radical can, in principle, isomerize to 3-tolyl and/or 2-tolyl and also to the thermodynamically more stable benzyl radical ($C_6H_5CH_2$). However, even the lowest energy barrier for such isomerization would require 180 kJ mol^{-1},[48] which is too high for the available energy under our experimental conditions (single photon dissociation). Photodissociation experiments similar to our conditions at 193 nm have been reported in the literature,[49,50] which measure two major channels with translational energies [67 kJ mol^{-1} (31%) and 130 kJ mol^{-1} (60%)] dissipating in the 4-tolyl radical.[50] Only about 2 kJ mol^{-1} of internal energy exits in the molecular beam (at 200–300 K) making it an insignificant factor. Hence, by subtracting these
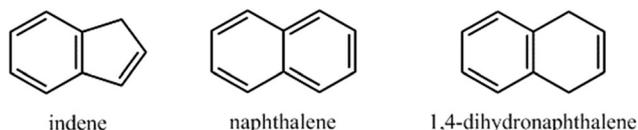

Fig. 1 PAH-like molecules formed in the reaction of phenyl radicals with distinct hydrocarbons: allene/methylacetylene, vinylacetylene, and 1,3-butadiene.

Table 1 Peak velocities (v_p), speed ratio (S), collision energy (E_c), and center-of-mass angles (Θ_{CM})

	v_p (ms^{-1})	S	E_c (kJ mol^{-1})	Θ_{CM}
C_5H_8 (isoprene)	710 ± 20	8.0 ± 0.2		
C_7H_7 (4-methyl phenyl)	1610 ± 40	7.5 ± 0.5	58.3 ± 1.5	18.3 ± 0.8

16806 | *Phys. Chem. Chem. Phys.*, 2014, **16**, 16805–16814

This journal is © the Owner Societies 2014

translational energies and C–Cl bond dissociation energy (407 kJ mol⁻¹)[50] from the photon energy, we obtain available energies as 146 kJ mol⁻¹ (31%) and 83 kJ mol⁻¹ (60%). The barriers for isomerization among 2-, 3- and 4-methylphenyl radicals are estimated to be about 260 kJ mol⁻¹.[48] Hence, this barrier is energetically not accessible in our experiments.

The neutral reaction products were analyzed using a triply differentially pumped rotatable mass spectrometer operated in the time-of-flight mode. Here, the neutral products are ionized by electron impact (80 eV, 2.0 mA), pass a quadrupole mass filter, and reach a Daly type ion detector operated at −22.5 kV.[51] The quadrupole mass spectrometer (Extrel QC 150) operated at 1.2 MHz and passed ions with the desired mass-to-charge, m/z, value. The signal from the photomultiplier tube passes a discriminator (Advanced Research Instruments, Model F-100TD, 1.5 mV) and is then fed into a Stanford Research System SR430 multichannel scaler to record the TOF spectrum.[46] These TOF spectra were recorded at multiple angles in the lab frame and then integrated to obtain the angular distribution of the product(s). A forward-convolution routine was used to fit the experimental data.[52,53] This iterative method initially assumes an angular flux distribution, $T(\theta)$, and the translational energy flux distribution, $P(E_T)$ in the center-of-mass (CM) system. Laboratory TOF spectra and the laboratory angular distributions (LAB) were then calculated from the $T(\theta)$ and $P(E_T)$ functions accounting for the velocity and angular spread of each beam. Best fits were obtained by iteratively refining the adjustable parameters in the center-of-mass system within the experimental error limits such as peak velocity, the speed ratio, and error bars in the LAB distribution. Finally, we obtained the product flux contour map, $I(\theta,u) = T(\theta) \times P(u)$, which represents the intensity of the reactive scattering products (I) as a function of the CM scattering angle (θ) and the product velocity (u) in the center-of-mass reference frame. This plot characterizes the reactive differential cross section and yields an image of the chemical reaction.

2.2. Computational

Geometries of all local minima structures and transition states on the $C_{12}H_{15}$ potential energy surface (PES) accessed by the reaction of the 4-methylphenyl radical with isoprene were optimized using the hybrid density functional B3LYP[54,55] method with the 6-311G** basis set. The same B3LYP/6-311G** method was applied to calculate zero-point energy (ZPE) corrections and vibrational frequencies required for further statistical theory calculations of rate constants of various reaction steps. Single-point energies were refined using the B3LYP optimized structures and utilizing a modified G3(MP2,CC)//B3LYP[56,57] approach according to the following formula:

$$E_0[\text{G3(MP2,CC)}] = E[\text{RCCSD(T)/6-311G*}] + \Delta E_{MP2} + \Delta E(\text{HLC})$$
$$+ E(\text{ZPE}),$$

where $\Delta E_{MP2} = E[\text{MP2/G3large}] - E[\text{MP2/6-311G*}]$ is a basis set correction, $\Delta E(\text{HLC})$ is a higher level correction, and $E(\text{ZPE})$ is the zero-point energy. $\Delta E(\text{HLC})$ was omitted in our calculations because all isomerization and dissociation steps of radical

species considered here proceed without a spin change resulting in HLC cancellation. The described calculation scheme represents a modification of the original G3[58] method and its expected accuracy for relative energies of hydrocarbon molecules and radicals, including transition states, is within 10 kJ mol⁻¹.[56,57] The CCSD(T) method which is central in the G3 scheme is recognized to be the gold standard for accurate calculations of molecules with single-reference or moderately multireference wave functions. The absence of a strong multireference character was monitored through T1 diagnostics in CCSD calculations and for all species considered the T1 diagnostic values did not exceed 0.02 indicating that their CCSD(T) energies should be reliable. All calculations were performed using GAUSSIAN 09[59] and MOLPRO 2010[60] program packages.

Rate constants $k(E)$ were computed using RRKM theory[61–63] taking the internal energy E as a sum of the energy of chemical activation in the 4-methylphenyl+isoprene reaction and a collision energy, with an assumption that a dominant fraction of the latter is converted to the internal vibrational energy. Multiwell–multichannel RRKM calculations were performed using a program developed for zero-pressure conditions relevant to single-collision conditions. The harmonic approximation was employed to calculate the total number and density of states. Product branching ratios were evaluated by solving first-order kinetic equations for unimolecular reactions within the steady-state approximation according to the kinetics scheme based on the *ab initio* potential energy diagram.

3. Experimental results

3.1. Laboratory frame

In the reaction of *para*-tolyl (C_7H_7; 91 amu) with isoprene (C_5H_8; 68 amu) the scattering signal was observed at mass-to-charge ratios (m/z) of 158 ($C_{12}H_{14}^+$) and 157 ($C_{12}H_{13}^+$). The signal at $m/z = 158$ ($C_{12}H_{14}^+$) proposes the existence of a 4-tolyl *versus* hydrogen atom exchange pathway leading to a product with the molecular formula $C_{12}H_{14}$. Note that the time-of-flight (TOF) spectra at $m/z = 158$ and 157 were indistinguishable after scaling; therefore, we can conclude that the signal at $m/z = 157$ originates from dissociative ionization of the $C_{12}H_{14}$ parent in the ionizer. The TOF spectra at $m/z = 158$ and the corresponding laboratory angular distribution are shown in Fig. 2 and 3, respectively. Here, the laboratory angular distribution is spread over at least 15° and depicts a forward–backward symmetry around the center-of-mass angle of 18°. This finding proposes that the reaction involves indirect, complex forming, scattering dynamics involving the decomposition of $C_{12}H_{15}$ complexes. Since both reactants contain a methyl group, we attempted to record data for possible methyl loss channel in the reaction at $m/z = 144$ ($C_{11}H_{12}$). The signal was observed; however, scaling and overlapping of TOFs at $m/z = 144$ with those recorded at $m/z = 158$ and 157 indicate that the signal at $m/z = 144$ originates from dissociative electron impact ionization of the $C_{12}H_{14}$ product. Further, we attempted to probe the adduct at $m/z = 159$ ($C_{12}H_{15}^+$); however, the intensity of the ion counts at $m/z = 159$ could be
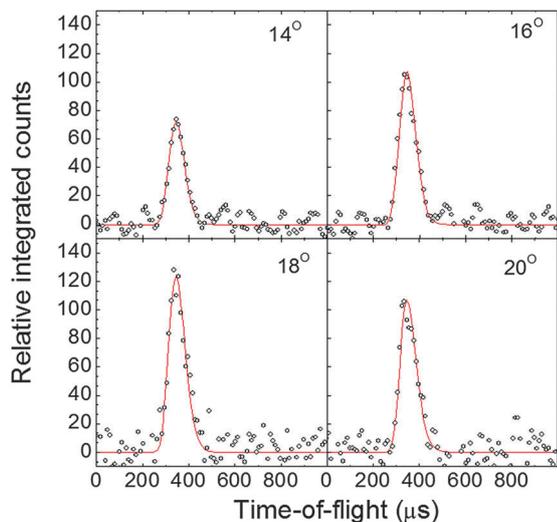
Fig. 2 Time-of-flight spectra collected at m/z = 158 for the reaction of the 4-methylphenyl radical with isoprene at collision energies of 58.3 ± 1.5 kJ mol^{-1}. Circles represent the experimental data and the solid lines represent the fit.

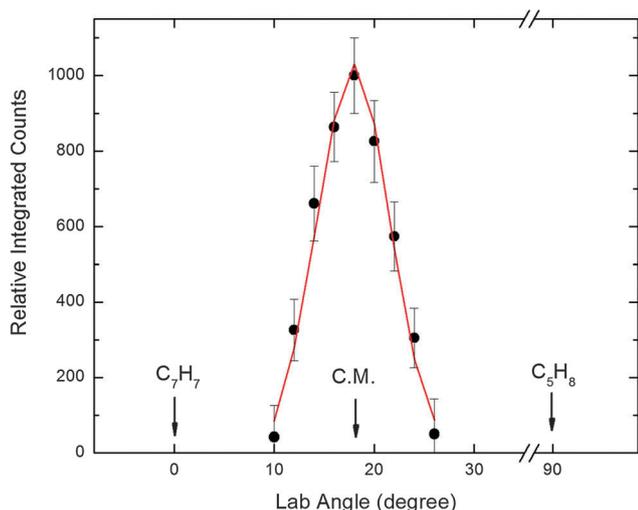Fig. 3 Laboratory angular distribution of the product recorded at m/z = 158. The center-of-mass angle is shown by C.M. Filled circles and 1σ error bars represent the experimental data, and the solid line represents the calculated distribution.
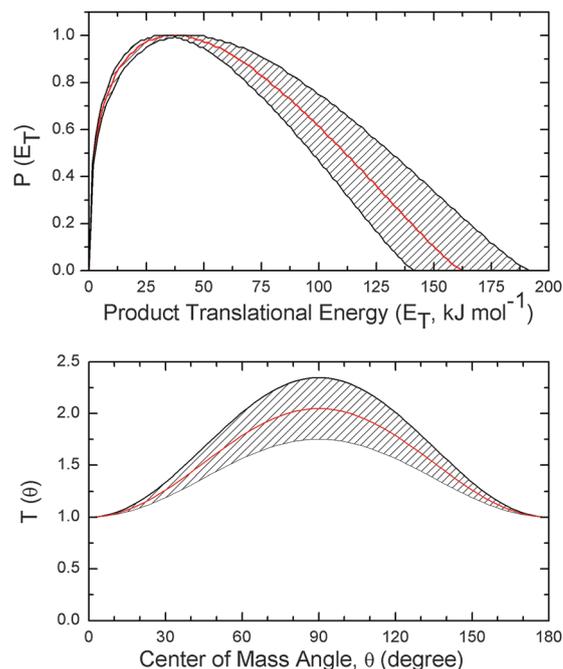

Fig. 4 Center-of-mass translational energy flux distribution (upper) and angular distribution (lower) for the hydrogen atom loss channel. Hatched areas indicate the acceptable upper and lower error limits of the fits and the solid red lines define the best-fit functions.

explained with the formation of ($^{13}CC_{11}H_{14}{}^{+}$), which is formed at levels of about 13% relative to the signal observed at $C_{12}H_{14}{}^{+}$ due to naturally occurring ^{13}C. Therefore, the analysis of the raw data alone proposes the formation of $C_{12}H_{14}$ isomers through an involvement of a 4-tolyl *versus* hydrogen atom exchange channel.

3.2. Center-of-mass frame

Having identified the molecular mass of the reaction product(s) as 158 amu ($C_{12}H_{14}$), we are attempting to extract the underlying reaction dynamics. For this, we convert the laboratory data into the center-of-mass reference frame and discuss the

resulting translational energy, $P(E_T)$, and angular, $T(\theta)$, distributions (Fig. 4). As shown in Fig. 4, the center-of-mass translational energy distribution, $P(E_T)$, extends up to maximum of 161 ± 22 kJ mol^{-1}. For those molecules born without internal excitation, this maximum presents the sum of reaction energy plus the collision energy. Subtracting nominal collision energy of 58 ± 2 kJ mol^{-1} from the maximum translational energy release, we determine the reaction exoergicity to be 103 ± 24 kJ mol^{-1}. Also, the $P(E_T)$ distribution peaks away from the zero translational energy depicting a broad maximum at 20–30 kJ mol^{-1}. This finding suggests the existence of at least one tight exit transition state for the decomposition of complex $C_{12}H_{15}$. In other words, the reverse reaction of hydrogen atom addition to the closed shell $C_{12}H_{14}$ molecule has an entrance barrier(s) of this magnitude. Finally, from the $P(E_T)$ distribution by integrating the translational energy distribution and accounting for the available energy, the average fraction of available energy channeling into the translational degrees of freedom is computed to be $36 \pm 4\%$. This order of magnitude indicates indirect scattering dynamics *via* complex formation in agreement with the conclusions drawn from the shape of the laboratory angular distribution as shown in Fig. 3.[64]

The center-of-mass angular distribution, $T(\theta)$, as depicted in Fig. 4, provides additional information on the reaction dynamics. It portrays intensity over the complete angular range from 0° to 180° indicating indirect scattering dynamics. Further, the forward–backward symmetry around 90° suggests that the life time of the intermediate(s) is longer than its (their) rotational period or that the reaction intermediate is 'symmetric'.[65] Finally, the distribution

16808 | *Phys. Chem. Chem. Phys.*, 2014, **16**, 16805–16814

This journal is © the Owner Societies 2014

maximum at 90° proposed geometrical constraints, *i.e.* an emission of the hydrogen atom almost parallel to the total angular momentum vector and nearly perpendicular to the rotational plane of the decomposing intermediate complex.[65]

4. Theoretical results

The potential energy surface (PES) for the reaction of the 4-tolyl radical with isoprene is presented in Fig. 5 and 6. Our computations identified ten reaction intermediates (**i1–i10**) and twelve possible reaction products (**p1–p12**) starting with the initial interaction of the 4-tolyl radical and the π electron density of the isoprene molecule and the barrier-less formation of a van-der-Waals complex (**i0**). Structures of the intermediates and products are shown in Scheme 1 while the complete list of Cartesian coordinates for all the reactants, intermediates, transition states and products is given in the ESI.† From **i0**, the addition to the C4 and C3 positions of isoprene leads to intermediates **i1** and **i4**, respectively, which are connected *via* a transition state located 117 kJ mol^{-1} above **i1**. Note that although both reactions involve barriers of 3 and 14 kJ mol^{-1}, the barrier to addition leading to intermediate **i1** resides *lower* than the energy of the separated reactants. This submerged barrier makes the addition of the 4-tolyl radical to the C4 position of isoprene *de facto* barrierless; the existence of a submerged

barrier was also monitored in the reactions of the phenyl radical with 1,3-butadiene (H$_2$CCHCHCH$_2$)[31] and vinylacetylene (H$_2$CCHCCH)[30] studied earlier in our group. Note that the van-der-Waals complex can also lead to hydrogen abstraction pathways at the C1, C3, C4, and the methyl group carbon atoms of isoprene, which can also be accessed directly from the separated reactants and from toluene (C$_6$H$_5$CH$_3$) plus distinct C$_5$H$_7$ radicals. However, the inherent barriers to abstraction of 11 to 35 kJ mol^{-1} relative to the reactants cannot compete with the *de facto* barrier-less addition to C4 – at least not at low collision energies and/or low temperatures of 10 K as found in cold molecular clouds. It is important to stress that toluene (92 amu) cannot be observed in our detector due to the inelastic scattering background from ^{13}C-4-tolyl, which is present at fractions of 7.7% relative to 4-tolyl in the primary beam. What is the future of intermediates **i1** and **i4**? Intermediate **i1** can isomerize to intermediates **i2** (by rotation around a single C–C bond), **i4** (by migration of the 4-methylpenyl group from C4 to C3), and **i5** (*via* ring closure). Considering the inherent barrier of 184 kJ mol^{-1} with respect to **i1**, the **i1** → **i5** pathway does not compete with the **i1** → **i2** and **i1** → **i4** isomerization, and **p5** is likely not formed in the reaction. Alternatively, **i1** can undergo unimolecular decomposition *via* atomic hydrogen elimination forming **p1** *via* a tight exit transition state. Once again, the barrier of 163 kJ mol^{-1} with respect to **i1** suggests that the **i1** → **i2** and **i1** → **i4** rearrangements are more favorable.

Fig. 5 Potential energy surface diagram for the addition of the 4-methylphenyl radical to the C3 and C4 carbon atoms of isoprene. Intermediates are labeled as **i** and products as **p**. All energies are relative to the separated reactants in kJ mol^{-1} as calculated at the G3(MP2,CC)//B3LYP/6-311G** +ZPE(B3LYP/6-311G**) levels of theory. Structures of the intermediates and products are given in Scheme 1.

This journal is © the Owner Societies 2014

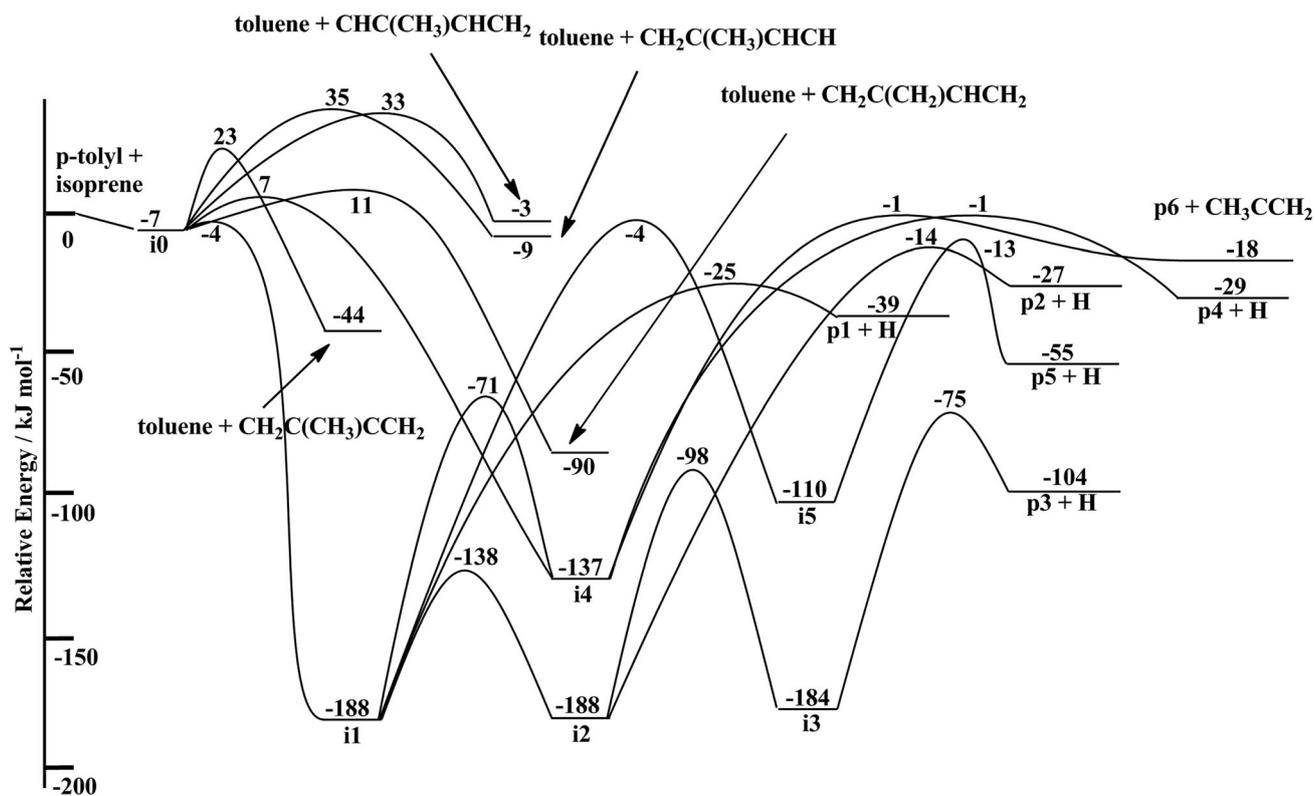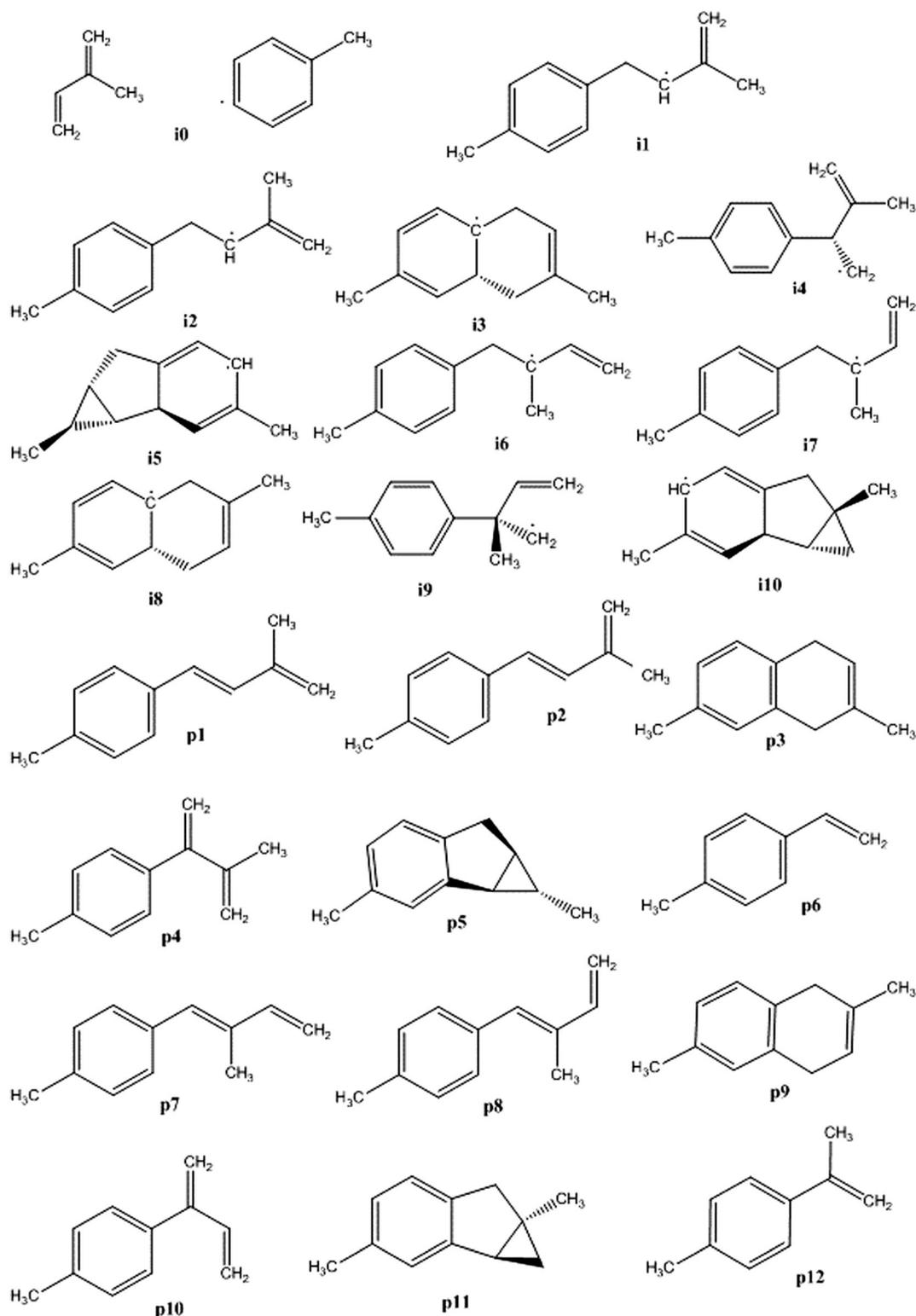*Phys. Chem. Chem. Phys.*, 2014, **16**, 16805–16814 | 16809

Fig. 6 Potential energy surface diagram for the addition of the 4-methylphenyl radical to the C1 and C2 carbon atoms of isoprene. Intermediates are labeled as **i** and products as **p**. All energies are relative to the separated reactants in kJ mol^{-1} as calculated at the G3(MP2,CC)//B3LYP/6-311G**+ZPE(B3LYP/6-311G**) levels of theory. Structures of the intermediates and products are given in Scheme 1.

Intermediate **i2** can either fragment *via* atomic hydrogen loss yielding **p2** or isomerizes *via* ring closure to **i3**. Considering the corresponding barriers of 174 and 90 kJ mol^{-1}, the **i2** → **i3** pathway followed by atomic hydrogen loss to 3,7-dimethyl-1,2-dihydronaphthalene (**p3**) is favorable. Note that **i4** also ejects a hydrogen atom from the former isoprene moiety to form **p4**; alternatively, the decomposition of **i4** can lead to **p6** (4-methyl-styrene) and 2-propenyl (CH$_3$CCH$_2$).

The addition of the 4-tolyl radical to the C1 and C2 positions of the isoprene (Fig. 6) is also preceded by the formation of the van-der-Waals complex (**i0**). This complex can then isomerize *via* addition to C1 and C2 leading to intermediates **i6** and **i9**, respectively. These intermediates are connected *via* a transition state located 119 kJ mol^{-1} above **i6**. Note that although both reactions involve barriers of 1 and 20 kJ mol^{-1}, the barrier to addition leading to intermediate **i6** resides *lower* than the energy of the separated reactants. This submerged barrier makes the addition of the 4-tolyl radical to the C1 position *de facto* barrier-less and favoring C1 addition compared to addition to C2. Intermediate **i9** can decompose to **p10** and **p12** by emitting a methyl (CH$_3$) and a vinyl group (C$_2$H$_3$), respectively. Intermediate **i6** can decompose to **p7** *via* hydrogen atom ejection without an exit barrier, might rearrange to **i7** *via* rotation around a single C–C bond through a barrier of only 56 kJ mol^{-1}, or ring close to **i10** *via* a barrier of 188 kJ mol^{-1}. **i10** then can emit a hydrogen atom forming **p11** by passing a tight exit transition state. **i7** can either lose a hydrogen atom to form **p8** or rearranges to **i8** *via* a lower barrier of 96 kJ mol^{-1} involving a ring closure. Finally, **i8** can emit a hydrogen atom from the 4-tolyl moiety to form 2,7-dimethyl-dihydronaphthaene

(**p9**) *via* a tight exit transition state, which is located at 30 kJ mol^{-1} above the separated products.

5. Discussion

We are merging now the experimental data with the computational results to gain insights into the underlying reaction dynamics and mechanisms. First, let us assign the structural isomer(s) formed. The experiments provide evidence on the formation of C$_{12}$H$_{14}$ molecules under single collision conditions. Further, the experimentally determined reaction energy was -103 ± 24 kJ mol^{-1}. A comparison of this data with the computed reaction energies proposes the formation of dimethyl-dihydronaphthalenes (**p3** and/or **p9**), *i.e.* the synthesis of the thermodynamically most stable C$_{12}$H$_{14}$ isomers. Based on the experimental data alone, we cannot exclude the formation of thermodynamically less stable isomers (**p1**, **p2**, **p4**, **p5**, **p7**, **p8**, **p11**). Based on the center-of-mass translational energy distribution, upper levels of 20% were derived for these products. How can the cyclic reaction products **p3** and **p9** be formed? We propose that the reaction proceeds *via* indirect (complex forming) scattering dynamics and is initiated by the formation of the van-der-Waals complex **i0**. Addition of the 4-tolyl radical to the C3 and C4 carbon atom form **i4** and **i1**, respectively, with **i4** being able to isomerize to **i1**. This can be followed by the reaction sequence **i1** → **i2** → **i3** → **p3** *via* rotation around a single C–C bond, cyclization, and atomic hydrogen emission to form **p3**. An addition of 4-tolyl to C1 and C2 of isoprene leads to **i6** and **i9**, respectively, with the latter isomerizing easily to **i6**.

Scheme 1 Chemical structures of the intermediates and major products shown in Fig. 5 and 6.

This is followed by a similar reaction sequence through rotation around a single C–C bond, ring closure, and atomic hydrogen emission (i6 → i7 → i8 → p9) forming eventually p9. Both hydrogen emission pathways i3 → p3 and i8 → p9 involve tight exit transition states located 29 and 30 kJ mol^{-1} above the energy of the separated products. This is in line with the experimental results predicting tight exit transition states in the order of 20 to 30 kJ mol^{-1} based on the center-of-mass translational energy distribution.

This journal is © the Owner Societies 2014

Phys. Chem. Chem. Phys., 2014, 16, 16805–16814 | 16811
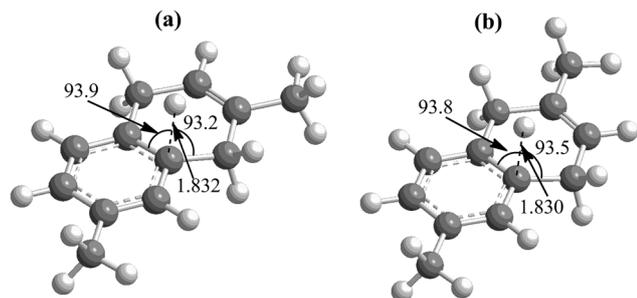
Fig. 7 Computed geometries of the exit transition states: (a) from inter-mediate **i3** to product **p3**, and (b) from intermediate **i8** to product **p9**.

Also note that the experiments and the shape of the center-of-mass angular distribution in particular predict that the hydrogen atom leaves perpendicular to the plane of the decomposing intermediate. Here, the geometry of the exit transition states (Fig. 7) leading to **p3** and **p9** supports this finding: the hydrogen atoms are emitted at angles of about 93° with respect to the molecular plane of the decomposing intermediates. Therefore, a comparison of the experimental data with the computations proposes the formation of the dimethyl-dihydronaphthalenes **p3** and/or **p9**. Finally, we exploited statistical calculations to predict the branching ratios assuming initial formation of the van-der-Waals complex **i0** followed by its unimolecular decomposition (Table 2). The RRKM calculations predict that at our experimental collision energy of 58 kJ mol^{-1}, **p9** and **p3** are the major products formed with branching ratios of 68.5% and 27.1%, respectively. Hence, all other products contribute only less than 5%. Consequently, we can conclude that the dimethyldihydronaphthalenes are the major products formed in our crossed molecular beam reaction. The reaction outcome is kinetically controlled and **p9** and **p3** appear to be the major products because their pathways, **i0** → **i6** → **i7** → **i8** → **p9** + H and **i0** → **i1** → **i2** → **i3** → **p3** + H, feature lower barriers than the routes to the other products. The branching ratio between the **p9** and **p3** products is controlled by branching of the reaction flux in the entrance channel, after the weak reactant complex **i0**, where, according to the calculated rate constants, the

formation of **i6** is a factor of ∼2.6 faster than the formation of **i1**. Even though our experimental collision energy translates to a high temperature (≈7000 K), it is important to note that, as shown in Table 2, the branching ratio only slightly depends on the collision energy from 0 to 60 kJ mol^{-1}. Hence, similar reaction dynamics can be expected for lower temperatures, such as those relevant to combustion. At low collision energies the ratio of the **p9** and **p3** product yields increases to a factor of ∼6. The result presented here is consistent with the reaction of the phenyl radical with 1,3-butadiene studied earlier in our group;[31] here the reaction was initiated by a barrierless addition of the phenyl radical to one of the terminal carbon atoms, followed by ring closure of the intermediate and hydrogen atom emission to 1,4-dihydronaphthalene (94%) at a collision energy of 55 kJ mol^{-1}. In other words, substitution of a methyl group at the C2 carbon of the 1,3-butadiene and in the phenyl radical does not influence the reaction mechanism, and the methyl groups act merely as spectators.

6. Conclusion

The crossed molecular beam reaction of the 4-methylphenyl radical with isoprene was investigated at a collision energy of 58 ± 2 kJ mol^{-1} under single collision conditions. Supplemented by the electronic structure calculations, the reaction was found to initially form a van-der-Waals complex without any entrance barrier, which can isomerize *via* addition of the 4-methylphenyl radical to any one of the four carbon atoms of the 1,3-butadiene moiety of isoprene. The initial addition products isomerize further, with C1 and C4 additions found to be formed preferentially. These intermediates undergo rotation around a single C–C bond, cyclization, and ultimately hydrogen atom elimination from the 4-methylphenyl moiety *via* tight exit transition states. Two dimethyl-dihydronaphthalene isomers were identified as the major products (95.6%). Ultimately, we have presented convincing evidence that methyl-substituted PAH-like molecules (here: dimethyl substituted and hydrogenated naphthalene molecules) can be formed *de facto* barrier-less (*via* a submerged barrier)

Table 2 Calculated branching ratios of the products for the reaction of *p*-tolyl radical with isoprene

| | Collision energies (kJ mol^{-1}) | | | | | | | | | | | | | |
	0	5	10	15	20	25	30	35	40	45	50	55	58	60
p1	0.00	0.00	0.00	0.00	0.00	0.00	0.00	0.01	0.01	0.01	0.02	0.03	0.03	0.03
p2	0.00	0.00	0.00	0.00	0.00	0.00	0.00	0.00	0.00	0.00	0.00	0.00	0.00	0.01
p3	14.14	19.42	21.89	23.35	24.32	25.09	25.57	25.99	26.33	26.60	26.83	27.02	27.11	27.16
p4	0.00	0.00	0.00	0.00	0.00	0.00	0.00	0.00	0.00	0.00	0.00	0.00	0.00	0.00
p5	0.00	0.00	0.00	0.00	0.00	0.00	0.00	0.00	0.00	0.00	0.00	0.00	0.00	0.00
p6	0.00	0.00	0.00	0.00	0.00	0.00	0.00	0.00	0.00	0.00	0.00	0.00	0.00	0.00
p7	0.02	0.04	0.07	0.12	0.19	0.30	0.44	0.62	0.86	1.16	1.62	1.97	2.27	2.50
p8	0.00	0.00	0.00	0.00	0.00	0.00	0.00	0.00	0.00	0.00	0.00	0.00	0.00	0.00
p9	85.62	80.31	77.77	76.18	75.02	74.00	73.22	72.41	71.61	70.80	69.85	69.03	68.46	68.06
p10	0.00	0.00	0.00	0.00	0.00	0.00	0.00	0.00	0.00	0.00	0.00	0.00	0.00	0.00
p11	0.00	0.00	0.00	0.00	0.00	0.00	0.00	0.00	0.00	0.00	0.00	0.00	0.00	0.00
p12	0.00	0.00	0.00	0.00	0.00	0.00	0.00	0.00	0.00	0.00	0.00	0.00	0.00	0.00
$CH_2C(CH_3)CCH_2$	0.01	0.01	0.01	0.01	0.02	0.02	0.03	0.03	0.04	0.06	0.07	0.09	0.10	0.11
$CH_2CHC(CH_3)CH$	0.00	0.00	0.00	0.00	0.00	0.00	0.00	0.00	0.00	0.00	0.01	0.01	0.01	0.01
$CH_2C(CH_3)CHCH$	0.00	0.00	0.00	0.00	0.00	0.00	0.00	0.00	0.00	0.00	0.00	0.00	0.00	0.00
$CH_2C(CH_2)CHCH_2$	0.21	0.21	0.26	0.33	0.44	0.58	0.75	0.94	1.14	1.37	1.60	1.85	2.01	2.12

in analogy to the reaction of the phenyl radical with 1,3-butadiene leading to dihydronaphthalene as studied earlier.

Acknowledgements

References

1   A. Kazakov and M. Frenklach, *Combust. Flame*, 1998, **112**, 270–274.

2   J. H. Seinfeld and J. F. Pankow, *Annu. Rev. Phys. Chem.*, 2003, **54**, 121–140.

3   A. G. G. M. Tielens, *Annu. Rev. Astron. Astrophys.*, 2008, **46**, 289–337.

4   P. J. Sarre, J. R. Miles and S. M. Scarrott, *Science*, 1995, **269**, 674–676.

5   L. J. Allamandola, D. M. Hudgins and S. A. Sandford, *Astrophys. J.*, 1999, **511**, L115–L119.

6   I. Cherchneff, *Astron. Astrophys.*, 2012, **545**, A12.

7   Z. H. Feng, W. W. Hu, W. N. Rom, M. Costa and M. S. Tang, *Carcinogenesis*, 2003, **24**, 771–778.

8   B. R. Stanmore, J. F. Brilhac and P. Gilot, *Carbon*, 2001, **39**, 2247–2268.

9   C. Baird, *Enviornmental Chemistry*, W. H. Freeman Company, New York, 1999.

10   D. G. Aubin and J. P. Abbatt, *J. Phys. Chem. A*, 2003, **107**, 11030–11037.

11   L. D. Sabin, K. Kozawa, E. Behrentz, A. M. Winer, D. R. Fitz, D. V. Pankratz, S. D. Colome and S. A. Fruin, *Atmos. Environ.*, 2005, **39**, 5243–5254.

12   B. J. FinlaysonPitts and J. N. Pitts, *Science*, 1997, **276**, 1045–1052.

13   K. Hylland, *J. Toxicol. Environ. Health, Part A*, 2006, **69**, 109–123.

14   S. Shantakumar, M. D. Gammon, S. M. Eng, S. K. Sagiv, M. M. Gaudet, S. L. Teitelbaum, J. A. Britton, M. B. Terry, A. Paykin, T. L. Young, L. W. Wang, Q. Wang, S. D. Stellman, J. Beyea, M. Hatch, D. Camann, B. Prokopczyk, G. C. Kabat, B. Levin, A. I. Alfred and R. M. Santella, *J. Exposure Anal. Environ. Epidemiol.*, 2005, **15**, 482–490.

15   P. Oleszczuk and S. Baran, *J. Environ. Sci. Health, Part A: Toxic/Hazard. Subst. Environ. Eng.*, 2005, **40**, 2085–2103.

16   W. C. Hinds, *Aerosol Technology: Properties, Behavior and Measurement of Airborne Particles*, Wiley, New York, 1999.

17   R. P. Wayne, *Chemistry of the Atmosphere*, Oxford University Press, Oxford, 2000.

18   D. M. Smith and A. R. Chughtai, *Colloids Surf., A*, 1995, **105**, 47–77.

19   T. Musafia-Jeknic, B. Mahadevan, C. Pereira and W. M. Baird, *Toxicol. Sci.*, 2005, **88**, 358–366.

20   D. U. Pedersen, J. L. Durant, K. Taghizadeh, H. F. Hemond, A. L. Lafleur and G. R. Cass, *Environ. Sci. Technol.*, 2005, **39**, 9547–9560.

21   D. M. Smith and A. R. Chughtai, *J. Atmos. Chem.*, 1997, **26**, 77–91.

22   M. Frenklach, *Phys. Chem. Chem. Phys.*, 2002, **4**, 2028–2037.

23   M. Frenklach and H. Wang, *Abstr. Pap. Am. Chem. Soc.*, 1991, **36**, 1509–1516.

24   U. Alkemade and K. H. Homann, *Z. Phys. Chem.*, 1989, **161**, 19–34.

25   N. Hansen, S. J. Klippenstein, J. A. Miller, J. Wang, T. A. Cool, M. E. Law, P. R. Westmoreland, T. Kasper and K. Kohse-Hoinghaus, *J. Phys. Chem. A*, 2006, **110**, 4376–4388.

26   M. M. Lu and J. A. Mulholland, *Chemosphere*, 2004, **55**, 605–610.

27   N. D. Marsh, M. J. Wornat, L. T. Scott, A. Necula, A. L. Lafleur and E. F. Plummer, *Polycyclic Aromat. Compd.*, 1999, **13**, 379–402.

28   M. Shukla, A. Susa, A. Miyoshi and M. Koshi, *J. Phys. Chem. A*, 2008, **112**, 2362–2369.

29   D. S. N. Parker, F. T. Zhang, R. I. Kaiser, V. V. Kislov and A. M. Mebel, *Chem. – Asian J.*, 2011, **6**, 3035–3047.

30   D. S. N. Parker, F. T. Zhang, Y. S. Kim, R. I. Kaiser, A. Landera, V. V. Kislov, A. M. Mebel and A. G. G. M. Tielens, *Proc. Natl. Acad. Sci. U. S. A.*, 2012, **109**, 53–58.

31   R. I. Kaiser, D. S. Parker, F. Zhang, A. Landera, V. V. Kislov and A. M. Mebel, *J. Phys. Chem. A*, 2012, **116**, 4248–4258.

32   T. C. Zhang, L. D. Zhang, X. Hong, K. W. Zhang, F. Qi, C. K. Law, T. H. Ye, P. H. Zhao and Y. L. Chen, *Combust. Flame*, 2009, **156**, 2071–2083.

33   G. da Silva, J. A. Cole and J. W. Bozzelli, *J. Phys. Chem. A*, 2010, **114**, 2275–2283.

34   L. Ackermann, H. Hippler, P. Pagsberg, C. Reihs and J. Troe, *J. Phys. Chem.*, 1990, **94**, 5247–5251.

35   L. B. Harding, S. J. Klippenstein and Y. Georgievskii, *J. Phys. Chem. A*, 2007, **111**, 3789–3801.

36   T. Ebata, K. Obi and I. Tanaka, *Chem. Phys. Lett.*, 1981, **77**, 480–483.

37   H. H. Nelson and J. R. Mcdonald, *J. Phys. Chem.*, 1982, **86**, 1242–1244.

38   K. Brezinsky, T. A. Litzinger and I. Glassman, *Int. J. Chem. Kinet.*, 1984, **16**, 1053–1074.

39   U. Brand, H. Hippler, L. Lindemann and J. Troe, *J. Phys. Chem.*, 1990, **94**, 6305–6316.

40   R. J. Kominar, M. G. Jacko and S. J. Price, *Can. J. Chem.*, 1967, **45**, 575–578.

41   R. Smith, *J. Phys. Chem.*, 1979, **83**, 1553–1563.

42   M. Rossi and D. M. Golden, *J. Am. Chem. Soc.*, 1979, **101**, 1230–1235.

43   G. da Silva, C. C. Chen and J. W. Bozzelli, *J. Phys. Chem. A*, 2007, **111**, 8663–8676.

44   J. G. Burr and J. D. Strong, *J. Chem. Phys.*, 1965, **43**, 1432–1433.

45   T. Ichimura, Y. Mori, M. Sumitani and K. Yoshihara, *J. Chem. Phys.*, 1986, **84**, 1943–1944.

46   Y. Guo, X. Gu, E. Kawamura and R. I. Kaiser, *Rev. Sci. Instrum.*, 2006, **77**, 034701.

47   R. I. Kaiser, P. Maksyutenko, C. Ennis, F. T. Zhang, X. B. Gu, S. P. Krishtal, A. M. Mebel, O. Kostko and M. Ahmed, *Faraday Discuss.*, 2010, **147**, 429–478.

This journal is © the Owner Societies 2014

Phys. Chem. Chem. Phys., 2014, **16**, 16805–16814 | **16813**

48 E. Dames and H. Wang, *Proc. Combust. Inst.*, 2013, **34**, 307–314.

49 T. Ichimura, Y. Mori, H. Shinohara and N. Nishi, *Chem. Phys. Lett.*, 1985, **122**, 55–58.

50 T. Ichimura, Y. Mori, H. Shinohara and N. Nishi, *J. Chem. Phys.*, 1997, **107**, 835–842.

51 N. R. Daly, *Rev. Sci. Instrum.*, 1960, **31**, 264–267.

52 M. Vernon, PhD thesis, University of California, Berkeley (Berkeley, CA), 1981.

53 P. S. Weiss, PhD thesis, University of California, Berkeley (Berkeley, CA), 1986.

54 A. D. Becke, *J. Chem. Phys.*, 1993, **98**, 5648–5652.

55 C. T. Lee, W. T. Yang and R. G. Parr, *Phys. Rev. B: Condens. Matter Mater. Phys.*, 1988, **37**, 785–789.

56 A. G. Baboul, L. A. Curtiss, P. C. Redfern and K. Raghavachari, *J. Chem. Phys.*, 1999, **110**, 7650–7657.

57 L. A. Curtiss, K. Raghavachari, P. C. Redfern, A. G. Baboul and J. A. Pople, *Chem. Phys. Lett.*, 1999, **314**, 101–107.

58 L. A. Curtiss, K. Raghavachari, P. C. Redfern, V. Rassolov and J. A. Pople, *J. Chem. Phys.*, 1998, **109**, 7764–7776.

59 M. J. Frisch, *et al.*, *Gaussian 09*, 2009.

60 H.-J. Werner, P. J. Knowles, G. Kinizia, F. R. Manby, M. Schutz, P. Celani, T. Korona and R. Lindh, 2010, *Molpro, version 2010.1*, a package of ab initio programs, http://molpro.net.

61 H. Eyring, S. H. Lin and S. M. Lin, *Basis Chemical Kinetics*, Wiley, New York, 1980.

62 P. J. Robinson and K. A. Holbrook, *Unimolecular Reactions*, Wiley Interscience, London, 1972.

63 J. I. Steinfeld, J. S. Francisco and W. L. Hase, *Chemical Kinetics and Dynamics*, Prentice Hall, New Jersey, 2nd edn, 1999.

64 W. B. Miller, S. A. Safron and D. R. Herschbach, *Discuss. Faraday Soc.*, 1967, **44**, 108–122.

65 R. D. Levine, *Molecular Reaction Dynamics*, Cambridge University Press, Cambridge, UK, 2005, pp. 138–141.